

THE ANISOTROPIC TRUNCATED KERNEL METHOD FOR CONVOLUTION WITH FREE-SPACE GREEN'S FUNCTIONS

LESLIE GREENGARD*, SHIDONG JIANG[†], AND YONG ZHANG[‡]

Abstract. A common task in computational physics is the convolution of a translation invariant, free-space Green's function with a smooth and compactly supported source density. Fourier methods are natural in this context, but encounter two difficulties. First, the kernel is typically singular in Fourier space and second, the source distribution can be highly anisotropic. The truncated kernel method [49] overcomes the first difficulty by taking into account the spatial range over which the solution is desired and setting the Green's function to zero beyond that range in a radially symmetric fashion. The transform of this truncated kernel can be computed easily and is infinitely differentiable by the Paley-Wiener theorem. As a result, a simple trapezoidal rule can be used for quadrature, the convolution can be implemented using the FFT, and the result is spectrally accurate.

Here, we develop an anisotropic extension of the truncated kernel method, where the truncation region in physical space is a rectangular box, which may have a large aspect ratio. In this case, the Fourier transform of the truncated kernel is again smooth, but is typically not available analytically. Instead, an efficient sum-of-Gaussians approximation is used to obtain the Fourier transform of the truncated kernel efficiently and accurately. This then permits the fast evaluation of the desired convolution with a source distribution sampled on an anisotropic, tensor-product grid. For problems in d dimensions, the storage cost is $O(2^d N)$ independent of the aspect ratio, and the computational cost is $O(2^d N \log(2^d N))$, where N is the total number of grid points needed to resolve the density. The performance of the algorithm is illustrated with several examples.

Key words. Truncated kernel method, sum-of-Gaussian approximation, anisotropic density, FFT, Green's function

AMS subject classifications. 68Q25, 68R10, 68U05

1. Introduction. In this paper, we consider the evaluation of convolution integrals of the form

$$(1.1) \quad \phi(\mathbf{x}) = [U * \rho](\mathbf{x}) = \int_{\mathbb{R}^d} U(\mathbf{x} - \mathbf{y})\rho(\mathbf{y})d\mathbf{y},$$

where d is the ambient dimension, $\rho(\mathbf{x})$ is a smooth and compactly supported (or rapidly decaying) source distribution, and the convolution kernel $U(\mathbf{x})$ is a known radially symmetric function, which might be singular at the origin and/or at infinity. A typical example is the solution of the Poisson equation

$$-\Delta\phi = \rho$$

in free space, in which case $U(\mathbf{x}) = -\frac{1}{2\pi} \ln|\mathbf{x}|$ for $d = 2$ and $U(\mathbf{x}) = \frac{1}{4\pi|\mathbf{x}|}$ for $d = 3$.

It is well known from the convolution theorem that $\phi(\mathbf{x})$ in (1.1) can be computed

*Courant Institute of Mathematical Sciences, New York University, NY, United States and Flatiron Institute, Simons Foundation, New York, NY, United States, (greenard@cims.nyu.edu).

[†]Department of Mathematical Sciences, New Jersey Institute of Technology, Newark, New Jersey, 07102, USA (shidong.jiang@njit.edu). S. Jiang was supported by the National Science Foundation under grant DMS-1720405 and by the Flatiron Institute, a division of the Simons Foundation.

[‡] Center for Applied Mathematics, Tianjin University, Tianjin 300072, China; Wolfgang Pauli Institute c/o Fak. Mathematik, University Wien, Oskar-Morgenstern-Platz 1, 1090 Vienna, Austria, (sunny5zhang@gmail.com). Y. Zhang was supported by Schrödinger Fellowship J3784-N32, the Austrian Science Foundation (FWF) under grant No. F41 (SFB "VICOM"), grant No. F65 (SFB "Complexity in PDEs") and the Wiener Wissenschafts und TechnologieFonds (WWTF) project No. MA16-066 ("SEQUEX").

35 in Fourier space by the formula

$$36 \quad (1.2) \quad \phi(\mathbf{x}) = \frac{1}{(2\pi)^d} \int_{\mathbb{R}^d} \widehat{U}(\mathbf{k}) \widehat{\rho}(k) e^{i\mathbf{k}\cdot\mathbf{x}} d\mathbf{k},$$

37 where the Fourier transform of f is defined as $\widehat{f}(\mathbf{k}) = \int_{\mathbb{R}^d} f(\mathbf{x}) e^{-i\mathbf{k}\cdot\mathbf{x}} d\mathbf{x}$. For the
38 Coulomb potential (the Poisson equation), we have

$$39 \quad (1.3) \quad \widehat{U}(\mathbf{k}) = \frac{1}{|\mathbf{k}|^2}.$$

40 This is, of course, true more generally; for any of the constant-coefficient partial dif-
41 ferential equations of mathematical physics, the solution due to a source distribution
42 $\rho(\mathbf{x})$ takes the form (1.1), (1.2), where $U(\mathbf{x})$ is the corresponding free-space Green's
43 function. Important cases aside from the Coulomb potential include the Yukawa
44 potential, the biharmonic potential, etc.

45 There is a substantial literature on alternative methods for the solution of partial
46 differential equations in free space. Finite difference and finite element discretization
47 of the governing equation, for example, are more flexible in terms of spatial adaptiv-
48 ity, but require the solution of large linear systems and the imposition of artificial,
49 “outgoing” boundary conditions on the boundary of a finite computational domain.
50 Integral transform methods, which compute (1.1) directly, avoid the need to *solve*
51 a linear system or to impose artificial boundary conditions, but require quadrature
52 schemes to handle the singularity of the kernel $U(\mathbf{x})$ and fast algorithms (such as
53 the fast Fourier transform or the fast multipole method) to reduce the $O(N^2)$ cost,
54 where N is the number of source and target points of interest (see, for example,
55 [1, 2, 7, 14, 16, 23, 30, 33, 34, 37]).

56 Here, we are interested in the development of purely Fourier-based methods,
57 sacrificing spatial adaptivity, but exploiting the speed of the FFT. The principal
58 novelty of the present work is that we develop an effective method for the case where
59 the source term ρ is strongly anisotropic, a situation which is frequently encountered
60 in confined quantum systems [3, 4]. More precisely, we seek to develop an efficient
61 method for (1.2) when ρ is given on a rectangular domain in d dimensions of the form

$$62 \quad (1.4) \quad \mathbf{R}_{L\gamma} = \prod_{j=1}^d [-L\gamma_j, L\gamma_j].$$

63 We define the *anisotropy vector* by $\gamma = (\gamma_1, \dots, \gamma_d)$. The magnitudes of the γ_j reflect
64 the degree of anisotropy. Without loss of generality, we assume that $\gamma_1 = 1$ and that
65 $\gamma_j \leq 1$ for $j = 2, \dots, d$. We also assume, for the sake of simplicity, that ρ is sampled
66 on a grid with the same number of points in each linear dimension (achieving greater
67 spatial resolution in the dimensions where γ_j is small).

68 DEFINITION 1.1. *We will refer to*

$$69 \quad (1.5) \quad \gamma_f := \prod_{j=2}^d \gamma_j^{-1}$$

70 *as the anisotropy factor. In the isotropic case, $\gamma_f = 1$, while for highly anisotropic*
71 *source distributions, $\gamma_f \gg 1$.*

72 Leaving anisotropy aside for the moment, suppose that we approximate the inte-
 73 gral in (1.2) by the trapezoidal rule (leading to a discrete Fourier transform). This,
 74 unfortunately, yields low order accuracy for the Poisson equation, because of the sin-
 75 gularity in the kernel (1.3) (see [5, 6, 18]). While Jiang *et al.* developed a high order
 76 correction method in three dimensions that uses a spherical coordinate system near
 77 the origin [27], it requires the use of the nonuniform FFT (NUFFT) [15, 24]. This
 78 approach has been extended successfully to a variety of other kernels [6, 36], includ-
 79 ing the 2D Poisson kernel, where the $1/|\mathbf{k}|^2$ singularity cannot be obviated by simply
 80 changing to polar coordinates. Nevertheless, the needed modifications can become
 81 rather complicated when dealing with more general kernels, such as the Helmholtz
 82 kernel, where singularities are not restricted to the origin. Moreover, significant work
 83 would be required to extend these methods to the case of anisotropic grids.

84 A simpler and more efficient method is described in the recent paper by Vico *et*
 85 *al.* [49], which we refer to as the truncated kernel method (TKM). It is based on the
 86 observation that, if one seeks the solution to the convolution equation (1.2) only in a
 87 ball B of radius R , with the source distribution supported in B as well, then no error
 88 is incurred by convolving with $U_B(\mathbf{x})$ instead of $U(\mathbf{x})$, where

$$89 \quad U_B(\mathbf{x}) = \begin{cases} U(\mathbf{x}) & \text{for } |\mathbf{x}| \leq 2R \\ 0 & \text{for } |\mathbf{x}| > 2R. \end{cases}$$

90 This is clear from inspection of the formula (1.1); the maximum distance of a target
 91 point of interest from a source point is $2R$. The truncated kernel $U_B(\mathbf{x})$ is compactly
 92 supported, so that $\widehat{U}_B(\mathbf{k})$ is entire (and C^∞) by the Paley-Wiener Theorem (see, for
 93 example, [44]). It is, in fact, straightforward to show that

$$94 \quad (1.6) \quad \widehat{U}_B(\mathbf{k}) = \frac{1 - \cos(2|\mathbf{k}|R)}{|\mathbf{k}|^2}.$$

95 In short, the TKM replaces (1.2) with

$$96 \quad (1.7) \quad \phi(\mathbf{x}) = \frac{1}{(2\pi)^d} \int_{\mathbb{R}^d} \widehat{U}_B(\mathbf{k}) \widehat{\rho}(\mathbf{k}) e^{i\mathbf{k}\cdot\mathbf{x}} d\mathbf{k}.$$

97 Note that for the source distribution in (1.4), we have

$$98 \quad (1.8) \quad R = L\sqrt{1 + \gamma_1^2 + \cdots + \gamma_d^2}.$$

99 Although smooth, \widehat{U}_B decays slowly in the Fourier domain. It is the smoothness
 100 of the source distribution that provides the needed high-frequency cut-off in (1.2).
 101 Combining these observations, it follows that trapezoidal rule discretization of (1.7)
 102 and the FFT lead to a spectrally accurate method. This idea was introduced in the
 103 Coulomb setting as the “supercell” method [26, 43], and in the Helmholtz setting by
 104 Vainikko [48]. The TKM [49] developed this approach in some generality and derived
 105 analytic formulas for $\widehat{U}_B(\mathbf{k})$ in connection with many physically important problems
 106 including the Coulomb, Helmholtz, biharmonic, and constant-coefficient advection-
 107 diffusion kernels in both two and three dimensions. It has recently been extended to
 108 systems with periodicity in a subset of directions in [45].

109 Returning now to the issue of anisotropy, let us assume that the source ρ is re-
 110 solved in physical space with a grid whose grid spacing in the j th coordinate direction
 111 is $\Delta x_j = L\gamma_j/n$. By standard results in Fourier analysis [47], it follows that

$$112 \quad (1.9) \quad \Delta k_j = \frac{\pi}{L\gamma_j}$$

113 is sufficient to resolve $\widehat{\rho}(\mathbf{k})$. Using the TKM, however, we would first need to enclose
 114 the rectangular box $\mathbf{R}_{L\gamma}$ from (1.4) in a sphere. As noted above, however, the radius
 115 of the smallest such sphere is given by (1.8) in d dimensions and the isotropically
 116 truncated kernel \widehat{U}_B requires that

$$117 \quad (1.10) \quad \Delta k_j < \frac{\pi}{2R}$$

118 in each coordinate direction. This can be seen either from inspection of the $\cos(2|\mathbf{k}|R)$
 119 term in (1.6) and the Nyquist-Shannon sampling theorem or from consideration of
 120 “local-global duality” in the Fourier transform [47]. As a result, to reach the desired
 121 resolution requires a factor of γ_f more points in Fourier space than needed to resolve
 122 the source distribution itself. A further oversampling factor of 2^d is needed in order to
 123 carry out aperiodic convolution (but that holds for any FFT-based scheme). In short,
 124 the excessively fine Δk_j needed to resolve $\widehat{U}_B(\mathbf{k})$ in (1.10) compared to that needed
 125 to resolve $\widehat{\rho}(\mathbf{k})$ in (1.9) makes the TKM prohibitively expensive for highly anisotropic
 126 problems.

127 In this paper, we propose an anisotropic truncated kernel method (ATKM) to
 128 handle anisotropic problems while avoiding the extra cost induced by the anisotropy
 129 factor γ_f . Instead of truncating the convolution kernel in a radially symmetric fashion,
 130 we set the kernel to zero outside a rectangular box that is twice the size of $\mathbf{R}_{L\gamma}$ in each
 131 direction. That is, we let $U_R(\mathbf{x}) = U(\mathbf{x})\chi_{\mathbf{R}_{2L\gamma}}(\mathbf{x})$. Since the truncated kernel $U_R(\mathbf{x})$
 132 now has the same anisotropic structure as the source ρ , this eliminates the need for
 133 uniform sampling in Fourier space when computing the inverse Fourier transform in
 134 (1.7). On the other hand, the truncated kernel in the Fourier domain now takes the
 135 form

$$136 \quad (1.11) \quad \widehat{U}_R(\mathbf{k}) = \int_{\mathbb{R}^d} U_R(\mathbf{x})e^{-i\mathbf{k}\cdot\mathbf{x}}d\mathbf{x} = \int_{\mathbf{R}_{2L\gamma}} U(\mathbf{x})e^{-i\mathbf{k}\cdot\mathbf{x}}d\mathbf{x}, \quad \mathbf{k} \in \mathbb{R}^d.$$

137 It no longer has an explicit analytical expression, even if the original kernel is radially
 138 symmetric. Instead, it must be computed numerically. For this, we approximate the
 139 kernel $U(\mathbf{x})$ by a sum of Gaussians $U_{GS}(\mathbf{x})$ for $|\mathbf{x}| \in [\delta, 2R]$, where δ is a cut-off
 140 parameter to be determined and R is given by (1.8).

141 That is, for a prescribed precision ε , we assume that

$$142 \quad (1.12) \quad \|U(\mathbf{x}) - U_{GS}(\mathbf{x})\| < \varepsilon\|U(\mathbf{x})\|, \quad \delta \leq |\mathbf{x}| \leq 2R,$$

143 where

$$144 \quad (1.13) \quad U_{GS}(\mathbf{x}) = \sum_{i=1}^S w_i e^{-s_i|\mathbf{x}|^2}.$$

145 We may then write

$$146 \quad (1.14) \quad \widehat{U}_R(\mathbf{k}) = \int_{\mathbf{R}_{2L\gamma}} U_{GS}(\mathbf{x})e^{-i\mathbf{k}\cdot\mathbf{x}}d\mathbf{x} + \int_{\mathbf{B}_\delta} [U(\mathbf{x}) - U_{GS}(\mathbf{x})]e^{-i\mathbf{k}\cdot\mathbf{x}}d\mathbf{x} + O(\varepsilon),$$

147 where \mathbf{B}_δ is the ball of radius δ .

148 It remains to find an efficient sum of Gaussians approximation for the first integral
 149 in (1.14) and a suitable asymptotic method to compute the second integral. We can
 150 then provide a complete description of the algorithm.

151 REMARK 1. *The approximation of the convolution kernel in physical space by*
 152 *a sum of Gaussians has been studied extensively in [10, 11, 9, 12, 17, 20, 21, 25,*
 153 *35]. The paper [17], in particular, is closely related to the present work. There, the*
 154 *convolution is split into a singular near-field component, computed using a Taylor*
 155 *expansion of the density and a regular far-field component, computed using a sum-of-*
 156 *Gaussians approximation of the kernel. Both can be evaluated via the FFT.*

157 REMARK 2. *The reason a sum-of-Gaussians approximation is particularly useful is*
 158 *that it permits the first (d -dimensional) integral in (1.14) to be computed as a product*
 159 *of d one-dimensional integrals - that is, it permits separation of variables. Thus, the*
 160 *cost of evaluating these one-dimensional integrals is only $O(SN^{1/d})$, where N is the*
 161 *total number of discretization points in either physical or Fourier space.*

162 *The cutoff parameter δ is chosen sufficiently small that a low-order asymptotic*
 163 *expansion yields sufficient accuracy and requires only $O(S+N)$ work for the evaluation*
 164 *of the second integral in (1.14).*

165 REMARK 3. *There have been other FFT based fast algorithms developed for the*
 166 *calculation of convolution-type integrals. These include the pre-corrected FFT for*
 167 *computing convolution integrals when the discretization points are close to but not*
 168 *exactly on a regular grid (see, for example, [40, 41, 50]) and Particle Mesh Ewald*
 169 *method for systems involving periodic conditions in certain directions (see, for exam-*
 170 *ple, [13, 31, 32, 46]). We do not intend to present a comprehensive review of these*
 171 *algorithms here, and refer the reader to the aforementioned references for details.*

172 The paper is organized as follows. We show, in section 2, that the number of
 173 Gaussians S is of the order $S = O(\log \delta \log \varepsilon)$ for a variety of non-oscillatory kernels
 174 with radial symmetry. In section 3, we present the ATKM with detailed error analysis
 175 and parameter selection strategies. In section 4, we illustrate the performance of the
 176 algorithm with several numerical examples. Some concluding remarks can be found
 177 in section 5.

178 **2. Sum-of-Gaussian approximation of convolution kernels.** In this sec-
 179 tion, we first consider the three-dimensional Yukawa (or modified Helmholtz) kernel
 180 $\frac{e^{-\lambda r}}{4\pi r}$, i.e., the Green's function for the partial differential equation $(-\Delta + \lambda^2)u = \rho$.
 181 The 3D Coulomb kernel (corresponding to $\lambda = 0$) and the general power function $\frac{1}{r^\beta}$
 182 with $\beta > 0$, have been studied in detail in [11].

183 We begin with the integral representation

$$184 \quad (2.1) \quad \frac{e^{-\lambda r}}{4\pi r} = \frac{1}{2\pi\sqrt{\pi}} \int_0^\infty e^{-r^2 t^2 - \frac{\lambda^2}{4t^2}} dt = \frac{1}{2\pi\sqrt{\pi}} \int_{\mathbb{R}} e^{-r^2 e^{2u}} e^{-\frac{\lambda^2}{4} e^{-2u}} e^u du,$$

185 where the first equality can be found in [8], and the second equality follows from
 186 change of variable $t = e^u$. The representation can be viewed as an integral of a
 187 Gaussian kernel with respect to the r variable so that a discrete sum-of-Gaussians
 188 approximation can be obtained by discretization.

189 LEMMA 2.1. *Let $[\delta, L]$ denote an interval with $0 < \delta < R$. Then*

$$190 \quad (2.2) \quad \left\| \frac{e^{-\lambda r}}{4\pi r} - U_{GS}(r) \right\| = O(e^{-C_1 M / \log M})$$

191 where

$$192 \quad (2.3) \quad U_{GS}(r) = \sum_{j=-M}^M \omega_j e^{-\tau_j^2 r^2},$$

193 with $\omega_j = \frac{1}{4\pi} \frac{2}{\sqrt{\pi}} h e^{u_j} e^{-\frac{\lambda^2}{4} e^{-2u_j}}$, $u_j = jh$, $\tau_j = e^{u_j}$, and $h = \log\left(\frac{2\pi aM}{b}\right)/(aM)$.

194 *Proof.* As a function of u , the integrand $f(u) := e^{-r^2 e^{2u}} e^{-\frac{\lambda^2}{4} e^{-2u}} e^u$ lies in $H^1(D_l)$
 195 for $l < \pi/2$ [25], containing all holomorphic functions in the strip $D_l := \{z \in \mathbb{C} : |\operatorname{Im} z| \leq l\}$,
 196 satisfying the additional property

$$197 \quad (2.4) \quad N(f, D_l) := \int_{\partial D_l} |f(z)| |dz| = \int_{\mathbb{R}} (|f(u+il)| + |f(u-il)|) du < \infty.$$

199 We also have that $|f(u)| \leq C e^{-be^{a|u|}}$ with $a = 2$, $b = \min\{\delta^2, \lambda^2/4\}$ for all $u \in \mathbb{R}$ and
 200 $r \in [\delta, R]$. Thus, by Proposition 2.1 in [25], the truncated trapezoidal rule applied to
 201 (2.1) leads to a spectrally accurate approximation. \square

202 **REMARK 4.** *In practice, we change the summation limits in (2.3) to M_1 and M_2*
 203 *by finding a range for u in (2.1) beyond which the integrand is negligible. We then*
 204 *apply standard model reduction algorithm (see, for example, [51]) to reduce the number*
 205 *of Gaussians as a final optimization step.*

206 **Table 2.1** shows the number of terms for various values of δ and ε over the interval
 207 $[\delta, 16\sqrt{3}]$ for $\lambda = 1$, where the desired accuracy ε is measured in the relative maximum
 208 norm. Note that the number of terms grows linearly (or sublinearly) in terms of both
 $\log(\varepsilon^{-1})$ and $\log(\delta^{-1})$.

TABLE 2.1

Number of Gaussians needed for approximating the 3D Yukawa kernel $U(r) = \frac{1}{4\pi} \frac{e^{-\lambda r}}{r}$ over
 $[\delta, 16\sqrt{3}]$ with $\lambda = 1$ for the given accuracy ε .

$\delta \setminus \varepsilon$	10^{-6}	10^{-7}	10^{-8}	10^{-9}	10^{-10}	10^{-11}	10^{-12}
10^{-3}	33	38	44	49	55	60	67
10^{-4}	40	46	53	60	67	73	80
10^{-5}	47	54	62	70	78	85	93
10^{-6}	54	62	72	80	90	98	107

209 For the 2D Yukawa kernel $\frac{1}{2\pi} K_0(\lambda r)$, where K_0 is the modified Bessel function
 210 of the second kind of order 0 (Section 10.25 in [39]), we may start from the integral
 212 representation (eq. 10.32.10 in [39])

$$213 \quad (2.5) \quad U_\lambda(r) = \frac{1}{2\pi} K_0(\lambda r) = \frac{1}{4\pi} \int_0^\infty e^{(-t - \frac{\lambda^2 r^2}{4t})} \frac{dt}{t} = \frac{1}{4\pi} \int_{\mathbb{R}} e^{-\frac{\lambda^2 r^2}{4} e^{-u}} e^{-e^u} du.$$

214 We then follow a similar procedure to obtain an efficient, accurate sum-of-Gaussians
 215 approximation.

216 **2.1. A black-box algorithm for the Gaussian-sum approximation of ra-**
 217 **dially symmetric kernels.** Assume now that the kernel is radially symmetric, i.e.,
 218 $U(\mathbf{x}) = U(r)$, $r = |\mathbf{x}|$. Then the problem is reduced to one-dimensional approximation
 219 problem. By a simple change of variable $r = \sqrt{x}$, we observe that the sum-of-Gaussian
 220 approximation of $U(r)$ on $[\delta, R]$ is equivalent to the sum-of-exponential approxima-
 221 tion of $U(\sqrt{x})$ on $[\delta^2, R^2]$. Sum-of-exponential approximations have been studied
 222 more extensively in literature (see, for example, [10, 11]). However, [10] samples the
 223 function using equispaced points; while [11] considers the power functions only. Here
 224 we consider sum-of-exponential approximation of a nonoscillatory function $f(x)$ on
 225 an interval $[a, b] \subset \mathbb{R}^+$. We assume that f is in general singular at the origin, as is

226 the case for most Green's functions, and the left end point a may be very close to
 227 the origin. Thus, the method in [10] does not seem to be a very effective method for
 228 finding sum-of-exponential approximation of f .

229 As is well known, the Laplace transform of an exponential function $e^{-\alpha t}$ is the pole
 230 function $\frac{1}{s+\alpha}$. In [51], a bootstrap method for finding sum-of-pole approximations for
 231 a certain class of function is developed. The method applies a nonlinear least squares
 232 procedure recursively on a successively larger interval on the imaginary axis. The
 233 method in [51] tries to find the sum-of-pole approximation for a given function such
 234 that the approximation is valid in the entire right half of the complex plane; while
 235 our objective here is to find a Gaussian-sum approximation on a finite interval.

236 We have developed a simplified algorithm for finding the sum-of-exponential ap-
 237 proximation. The algorithm consists of two stages (see [28] for details). In the first
 238 stage, a preliminary sum-of-exponential approximation that is accurate but inefficient
 239 is constructed for f on $[a, b]$. That is,

$$240 \quad (2.6) \quad f(x) \approx \sum_{j=1}^P \tilde{w}_j e^{\tilde{s}_j x}, \quad x \in [a, b].$$

241 This is done as follows. We first allocate a set of P logarithmically equally spaced
 242 points \tilde{s}_j ($j = 1, \dots, P$) lying on the negative real axis, which serve as the nodes in the
 243 preliminary sum-of-exponential approximation (2.6). Second, a set of sampling points
 244 on $[a, b]$ are constructed via adaptive bisections into smaller and smaller subintervals
 245 such that the given function f is accurately approximated by a Chebyshev polynomial
 246 of degree no greater than n_c on each subinterval. Since the origin is assumed to be a
 247 singular point, we further make dyadic subdivisions for the interval close to the origin.
 248 We denote these sampling points by x_i , $i = 1, \dots, M$. We now solve the following
 249 linear least squares problem

$$250 \quad (2.7) \quad A\tilde{w} = b,$$

251 where A is an $M \times P$ matrix with the entry $A_{ij} = e^{\tilde{s}_j x_i}$, \tilde{w} is a column vector of length
 252 P containing the weights in the preliminary sum-of-exponential approximation, and
 253 b is a column vector of length M with $b_i = f(x_i)$.

254 In the second stage, we apply the ‘‘squareroot method’’ in model reduction (see,
 255 for example, [51] and references therein for details) to reduce the number of exponen-
 256 tials to achieve a near optimal sum-of-exponential approximation. That is,

$$257 \quad (2.8) \quad \sum_{j=1}^P \tilde{w}_j e^{\tilde{s}_j x} \approx \sum_{j=1}^S w_j e^{s_j x}.$$

258 The optimality of the resulting sum-of-exponential approximation in L^∞ norm is
 259 guaranteed by well-known results in control theory (see, for example, [22]). We would
 260 like to remark that the model reduction technique was originally designed for sum-of-
 261 pole approximations. However, since all the nodes lie in the left half of the complex
 262 plane, we may apply it directly to the reduction of sum-of-exponential approximation
 263 due to the aforementioned connection between these two types of approximations.

264 Taking now $f(x) = U(\sqrt{x})$, $[a, b] = [\delta^2, R^2]$, and combining (2.6) and (2.8), we
 265 obtain

$$266 \quad (2.9) \quad U(\mathbf{x}) = U(r) = U(x) \approx \sum_{j=1}^S w_j e^{s_j x^2}, \quad x \in [\delta, R].$$

267 We have applied the algorithm to find efficient and accurate Gaussian-sum approxi-
 268 mations for many kernels, including the biharmonic Green's function in both two and
 269 three dimensions, the Poisson kernel in two dimensions, etc. The performance of the
 270 algorithm on these kernels is similar. Table 2.2 lists the number of Gaussians needed
 271 to approximate the 2D Poisson kernel $-\frac{1}{2\pi} \ln |\mathbf{x}|$ on the interval $[\delta, R]$ with various δ
 272 and relative L^2 error bound ε .

TABLE 2.2

Number of Gaussians needed for approximating the 2D Poisson kernel $U(r) = -\frac{1}{2\pi} \ln(r)$ over $[\delta, 2\sqrt{2}]$ for the given accuracy ε .

$\delta \setminus \varepsilon$	10^{-6}	10^{-7}	10^{-8}	10^{-9}	10^{-10}	10^{-11}	10^{-12}
10^{-3}	80	86	95	107	117	128	137
10^{-4}	98	109	124	136	152	160	171
10^{-5}	118	134	146	164	189	196	209
10^{-6}	131	151	167	195	214	231	241

273 **3. Anisotropic truncated kernel method.** We now discuss the ATKM in
 274 detail. We assume that the density function ρ is compactly supported in a generally
 275 anisotropic rectangular box $\mathbf{R}_{L\gamma}$ and well resolved by n equispaced points in each
 276 direction. Thus, the total number of grid points needed to resolve the density function
 277 ρ on $\mathbf{R}_{L\gamma}$ is $N = n^d$. We truncate the kernel on a rectangular box $\mathbf{R}_{2L\gamma}$ instead of
 278 an isotropic ball. That is,

$$279 \quad (3.1) \quad \begin{aligned} \phi(\mathbf{x}) &= \int_{\mathbb{R}^d} U(\mathbf{y})\rho(\mathbf{x} - \mathbf{y})d\mathbf{y} = \int_{\mathbf{x} + \mathbf{R}_{L\gamma}} U(\mathbf{y})\rho(\mathbf{x} - \mathbf{y})d\mathbf{y} \\ &= \int_{\mathbf{R}_{2L\gamma}} U(\mathbf{y})\rho(\mathbf{x} - \mathbf{y})d\mathbf{y}, \quad \mathbf{x} \in \mathbf{R}_{L\gamma}. \end{aligned}$$

280 For the density $\rho(\mathbf{x} - \mathbf{y})$ in (3.1), we have $\mathbf{x} - \mathbf{y} \in \mathbf{R}_{3L\gamma}$ for $\forall \mathbf{x} \in \mathbf{R}_{L\gamma}, \mathbf{y} \in \mathbf{R}_{2L\gamma}$.
 281 Therefore we can approximate the density ρ on $\mathbf{R}_{3L\gamma}$ by a Fourier pseudo-spectral
 282 method with spectral accuracy [47]. This seems to require a threefold zero-padding
 283 from $\mathbf{R}_{L\gamma}$ to $\mathbf{R}_{3L\gamma}$. However, straightforward analysis shows that to obtain the
 284 solution in the domain $\mathbf{R}_{L\gamma}$ itself, it is sufficient to carry out zero-padding to $\mathbf{R}_{2L\gamma}$.
 285 In short, the density ρ is well resolved by the following finite Fourier series

$$286 \quad (3.2) \quad \rho(\mathbf{z}) \approx \sum_{\mathbf{k}} \hat{\rho}_{\mathbf{k}} e^{i\mathbf{k} \cdot \mathbf{z}}, \quad \mathbf{z} \in \mathbf{R}_{2L\gamma},$$

287 where $\mathbf{k} = \frac{\pi}{2L} (\frac{k_1}{\gamma_1}, \dots, \frac{k_d}{\gamma_d})$ with $k_j = -n, \dots, n - 1$ for $j = 1, \dots, d$. The Fourier
 288 coefficients are given by the formula

$$289 \quad (3.3) \quad \hat{\rho}_{\mathbf{k}} = \frac{1}{|\mathbf{R}_{2L\gamma}|} \int_{\mathbf{R}_{2L\gamma}} \rho(\mathbf{z}) e^{-i\mathbf{k} \cdot \mathbf{z}} d\mathbf{z},$$

290 where $|\mathbf{R}_{2L\gamma}| = (4L)^d \prod_{j=1}^d \gamma_j$ is the volume of $\mathbf{R}_{2L\gamma}$.

291 By the assumption on ρ , the integral in (3.3) is well approximated by the trape-
 292 zoidal rule. Thus $\hat{\rho}_{\mathbf{k}}$ can be evaluated via the forward FFT of size $2^d N$. Using (3.1)
 293 and (3.2), we obtain

$$\begin{aligned}
\phi(\mathbf{x}) &= \int_{\mathbf{R}_{2L\gamma}} U(\mathbf{y})\rho(\mathbf{x} - \mathbf{y})d\mathbf{y} \\
294 \quad (3.4) \quad &\approx \sum_{\mathbf{k}} \hat{\rho}_{\mathbf{k}} e^{i\mathbf{k}\cdot\mathbf{x}} \left(\int_{\mathbf{R}_{2L\gamma}} U(\mathbf{y})e^{-i\mathbf{k}\cdot\mathbf{y}} d\mathbf{y} \right) \\
&:= \sum_{\mathbf{k}} \hat{U}_R(\mathbf{k}) \hat{\rho}_{\mathbf{k}} e^{i\mathbf{k}\cdot\mathbf{x}},
\end{aligned}$$

295 where $\hat{U}_R(\mathbf{k})$ is defined by the formula

$$296 \quad (3.5) \quad \boxed{\hat{U}_R(\mathbf{k}) := \int_{\mathbf{R}_{2L\gamma}} U(\mathbf{y})e^{-i\mathbf{k}\cdot\mathbf{y}} d\mathbf{y}.}$$

297 Clearly, once $\hat{U}_R(\mathbf{k})$ is available, the evaluation of the potential ϕ can be accom-
298 plished in three simple steps: (1) a forward FFT of size $2^d N$ for computing $\hat{\rho}(\mathbf{k})$, (2)
299 pointwise multiplication of $\hat{U}_R(\mathbf{k})$ and $\hat{\rho}(\mathbf{k})$, and (3) a backward FFT of size $2^d N$ for
300 computing $\phi(\mathbf{x})$. An alternative derivation of the procedure can be obtained from the
301 Fourier integral representation (1.2) rather than the convolution form to derive (3.4).
302 We prefer the derivation above because it is easier to verify that twofold zero-padding
303 along each direction is necessary and sufficient for the evaluation of the potential.

304 In order to compute $\hat{U}_R(\mathbf{k})$, we apply the Gaussian-sum approximation of the
305 kernel to split the integral into two parts as in (1.14). That is,

$$306 \quad (3.6) \quad \hat{U}_R(\mathbf{k}) \approx I_1(\mathbf{k}) + I_2(\mathbf{k}),$$

307 where

$$308 \quad (3.7) \quad I_2(\mathbf{k}) = \int_{B_\delta} (U - U_{GS})(\mathbf{y})e^{-i\mathbf{k}\cdot\mathbf{y}} d\mathbf{y}$$

309 and

$$\begin{aligned}
I_1(\mathbf{k}) &= \int_{\mathbf{R}_{2L\gamma}} U_{GS}(\mathbf{y})e^{-i\mathbf{k}\cdot\mathbf{y}} d\mathbf{y} = \int_{\mathbf{R}_{2L\gamma}} \sum_{i=1}^S w_i e^{s_i|\mathbf{y}|^2} e^{-i\mathbf{k}\cdot\mathbf{y}} d\mathbf{y} \\
310 \quad (3.8) \quad &= \sum_{i=1}^S w_i \prod_{j=1}^d G_{ij}(s_i, k_j),
\end{aligned}$$

311 with

$$312 \quad (3.9) \quad G_{ij}(s_i, k_j) = \int_{-2L\gamma_j}^{2L\gamma_j} e^{s_i y_j^2} e^{-\frac{\pi i k_j y_j}{2L\gamma_j}} dy_j, \quad i = 1, \dots, S, \quad k_j = -n, \dots, n-1.$$

313 The last equality in (3.8) follows from the separable structure of Gaussians. We
314 observe that the d -dimensional integral is decomposed into d one-dimensional Fourier
315 integrals of the Gaussians, leading to great reduction in the computational cost. Let
316 $\alpha^2 = -s_i L^2 \gamma_j^2$, $\beta = \pi k_j / 2$, and $x = y_j / (L\gamma_j)$. These one-dimensional integrals are

317 reduced to the following standard form

$$\begin{aligned}
\frac{G_{ij}(s_i, k_j)}{L\gamma_j} &= G(\alpha, \beta) = \int_{-2}^2 e^{-\alpha^2 x^2} e^{-i\frac{\pi k x}{2}} dx \\
318 \quad (3.10) \quad &= \frac{\sqrt{\pi}}{2\alpha} e^{-\frac{\beta^2}{4\alpha^2}} \left[\operatorname{erf}\left(2\alpha + i\frac{\beta}{2\alpha}\right) - \operatorname{erf}\left(-2\alpha + i\frac{\beta}{2\alpha}\right) \right] \\
&= \frac{\sqrt{\pi}}{\alpha} e^{-\frac{\beta^2}{4\alpha^2}} - \frac{\sqrt{\pi}}{\alpha} e^{-4\alpha^2} \operatorname{Re}\left(e^{-i\pi k_j \omega}\left(-\frac{\beta}{2\alpha} + 2i\alpha\right)\right).
\end{aligned}$$

319 Here $\operatorname{erf}(z) = \frac{2}{\sqrt{\pi}} \int_0^z e^{-t^2} dt$ is the error function [39] and $\omega(z) = e^{-z^2}(1 - \operatorname{erf}(-iz))$ is
320 the so-called Faddeeva function [19, 42, 52], which can be evaluated easily via existing
321 software package [29]. After the evaluation of these $2dSn = 2dSN^{1/d}$ one-dimensional
322 integrals, $I_1(\mathbf{k})$ can be evaluated in $O(S2^dN)$ multiplications and additions. Thus the
323 computation of $I_1(\mathbf{k})$ is very cheap, even though S may be in the order of 100. We
324 remark here that it is embarrassingly easy to parallelize this step, leading to further
325 reduction on the computational time if needed.

326 For $I_2(\mathbf{k})$, we expand the plane-wave function into Taylor series and calculate the
327 integral term by term. That is,

$$328 \quad (3.11) \quad I_2(\mathbf{k}) \approx \int_{B_\delta} (U - U_{\text{GS}})(\mathbf{y}) T(\mathbf{y}) d\mathbf{y},$$

329 where $T(\mathbf{y})$ is the truncated Taylor expansion of the complex exponential $e^{-i\mathbf{k}\cdot\mathbf{y}}$ of
330 order p . Since $U - U_{\text{GS}}$ is radially symmetric, any term involving $\mathbf{y}^\alpha := \prod_{j=1}^d y_j^{\alpha_j}$
331 with some odd α_j vanishes by symmetry. Hence, we only need to compute those even
332 power terms. The lowest order term is simply the integral of $U - U_{\text{GS}}$ itself. And the
333 second order terms can be calculated as follows

$$334 \quad (3.12) \quad \int_{B_\delta} (U - U_{\text{GS}})(\mathbf{y}) y_j^2 d\mathbf{y} = \frac{2^{d-1}\pi}{d} \int_0^\delta (U - U_{\text{GS}})(r) r^{d+1} dr.$$

335 This integral may be computed semianalytically for many kernels. For example, if U
336 is the 3D Coulomb kernel, then

$$337 \quad \int_{B_\delta} (U - U_{\text{GS}})(\mathbf{y}) y_j^2 d\mathbf{y} = \frac{4\pi}{3} \int_0^\delta \left(\frac{1}{4\pi r} - \sum_{i=1}^S w_i e^{s_i r^2} \right) r^4 dr = \frac{\delta^4}{12} - \frac{4\pi}{3} \sum_{i=1}^S w_i F(s_i, \delta),$$

338 where $F(s_i, \delta) = \int_0^\delta e^{s_i r^2} r^4 dr$. As k_j can be pulled out when evaluating these integrals,
339 the computational cost of evaluating $I_2(\mathbf{k})$ is $O(Sp + N)$ or simply $O(N)$ as $Sp \ll N$
340 in practice.

341 We now discuss the choice of the parameter δ . δ should be chosen so that the
342 truncation error of the Taylor expansion is uniformly bounded for all \mathbf{k} in the com-
343 putational range. That is, if we write

$$344 \quad (3.13) \quad E_T(\mathbf{k}) = \int_{B_\delta} (U - U_{\text{GS}})(\mathbf{y}) (e^{-i\mathbf{k}\cdot\mathbf{y}} - T(\mathbf{y})) d\mathbf{y},$$

345 where $T(\mathbf{y})$ is the Taylor expansion of the complex exponential $e^{-i\mathbf{k}\cdot\mathbf{y}}$ to the p -th
346 order, then we require that

$$347 \quad (3.14) \quad |E_T(\mathbf{k})| \leq \varepsilon$$

348 for all \mathbf{k} in the computational range. For the 3D Coulomb kernel, we have

349 (3.15)
$$|E_T(\mathbf{k})| = C \left(\frac{\pi |k| \delta}{2L\gamma_j} \right)^{p+4}, \quad |k| = 1, \dots, n, \quad j = 1, \dots, d.$$

350 Combining (3.14) and (3.15), we obtain

351 (3.16)
$$\delta \approx \frac{2L\varepsilon^{1/(p+4)}}{\pi N^{1/d}} \min_j \gamma_j.$$

352 For example, if $L = 8$, $p = 2$, $\varepsilon = 2 \times 10^{-16}$, $n = N^{1/d} = 128$, $\min_j \gamma_j = \frac{1}{16}$, then
 353 (3.16) leads to $\delta \approx 6 \times 10^{-6}$.

Algorithm 3.1 Anisotropic truncated kernel method

Comment: Given a precision requirement ε , the computational box $\mathbf{R}_{L\gamma}$, the convolution kernel U , and the density ρ , compute the potential defined in (1.1).

- 1: Precomputation stage: determine δ and find the Gaussian-sum approximation of the kernel U on $[\delta, 2R]$.
 - 2: Compute $2dSn$ one-dimensional integrals $G_{ij}(s_i, k_j)$ via (3.10).
 - 3: Compute $I_1(\mathbf{k})$ via (3.8).
 - 4: Compute $I_2(\mathbf{k})$ via (3.11).
 - 5: Compute the Fourier transform of the truncated kernel $\hat{U}_R(\mathbf{k})$ by adding $I_1(\mathbf{k})$ and $I_2(\mathbf{k})$.
 - 6: Compute $\hat{\rho}_{\mathbf{k}}$ via the forward FFT.
 - 7: Compute the product $\hat{U}_R(\mathbf{k})\hat{\rho}(\mathbf{k})$.
 - 8: Compute $\phi(\mathbf{x})$ via the backward FFT.
-

354 We summarize the algorithm in Algorithm 3.1. The second step requires $O(SN^{1/d})$
 355 work; the third step requires $O(SN)$ work; the fourth step requires $O(S + N)$ work;
 356 the fifth and seventh steps require $O(N)$ work; and the sixth and eighth steps require
 357 $O(N \log N)$ work. As noted before, S depends on δ and ε logarithmically. Combining
 358 this observation with (3.16), we have $S = O(\log N \log \varepsilon)$. Hence, the total computa-
 359 tional cost is $O(N \log N)$. Here we also note that the evaluation of $\hat{U}_R(\mathbf{k})$ (i.e., steps
 360 1–5 in the algorithm) need to be done only once for many time-dependent problems
 361 or problems with fixed geometry.

362 Finally, we would like to emphasize that the main advantage of the ATKM in
 363 this paper, as compared with the TKM in [49], is that one does not need excessive
 364 zero-padding for highly anisotropic problems. Figure 3.1 illustrates different zero-
 365 paddings of the TKM and the ATKM for an anisotropic density in two dimensions.
 366 The density $\rho(\mathbf{x})$ is assumed to be compactly supported in $\mathbf{R}_{L\gamma} = [-1, 1] \times [-\gamma, \gamma]$
 367 (here $\gamma = \frac{1}{4}$). The TKM in [49] requires that the physical domain be enlarged to
 368 $[-2, 2] \times [-2, 2]$ via zero-padding, i.e., a factor of $2^2/\gamma = 16$ increase in the number of
 369 discretization points. For the ATKM, the physical domain needs only to be enlarged
 370 to $[-2, 2] \times [-\frac{1}{2}, \frac{1}{2}]$, i.e., a factor of $2^2 = 4$ increase. The savings in the ATKM
 371 become even greater for three dimensional highly anisotropic problems. It should also
 372 be noted that the TKM requires an initialization phase with oversampling by a factor
 373 of 4 in each linear dimension rather than two [49]. This would increase the memory
 374 requirements, but can be obviated by decomposing the precomputation into smaller
 375 subproblems.

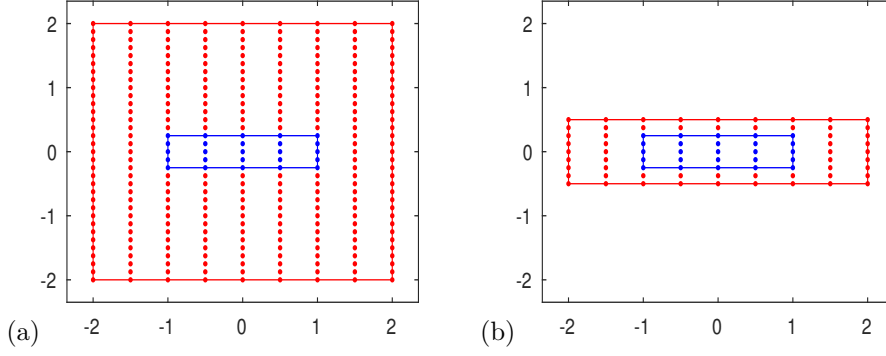


FIG. 3.1. Meshing strategies of the TKM (a) and the ATKM (b) for an anisotropic density $\rho(\mathbf{x})$ that is compactly supported in $[-1, 1] \times [-\frac{1}{4}, \frac{1}{4}]$ (labeled in blue). The zero-padded grid points are plotted in red. The zero-padded physical domain is $[-2, 2] \times [-2, 2]$ and $[-2, 2] \times [-\frac{1}{2}, \frac{1}{2}]$ for the TKM and the ATKM, respectively.

376 **3.1. Error estimates.** To derive error estimates of the algorithm, we only have
 377 to analyze the error of computing (3.5) via (3.6)–(3.11), as all other approximations
 378 are of spectral accuracy. Straightforward inspection shows that the error consists of
 379 two parts - the error due to the Gaussian-sum approximation of the kernel on $\mathbf{R}_{2L\gamma} \setminus B_\delta$
 380 and the error due to the truncated Taylor expansion of the complex exponential. That
 381 is

$$382 \quad (3.17) \quad E(\mathbf{k}) = E_{GS}(\mathbf{k}) + E_T(\mathbf{k}),$$

383 where $E_{GS}(\mathbf{k}) = \int_{\mathbf{R}_{2L\gamma} \setminus B_\delta} (U - U_{GS})(\mathbf{y}) e^{-i\mathbf{k} \cdot \mathbf{y}} d\mathbf{y}$ and $E_T(\mathbf{k})$ is given by (3.13). Using
 384 the Cauchy-Schwarz inequality, we have

$$385 \quad (3.18) \quad |E_{GS}(\mathbf{k})| \leq \int_{\mathbf{R}_{2L\gamma} \setminus B_\delta} |U - U_{GS}| d\mathbf{y} \leq S^{d-1} \int_\delta^{2R} |U - U_{GS}|(r) r^{d-1} dr \\ \leq \varepsilon \frac{S^{d-1}}{(2d-1)^{1/2}} \|U\|_{L^2([\delta, 2R])} (2R)^{d-1/2},$$

386 with $R = L\sqrt{\sum_j \gamma_j^2}$ and $S^{d-1} = \frac{2\pi^{d/2}}{\Gamma(d/2)}$. For $E_T(\mathbf{k})$, the choice of δ in (3.16) guaran-
 387 tees that $|E_T(\mathbf{k})| \leq \varepsilon$ for all \mathbf{k} in the computational range. Therefore, the error can
 388 be controlled to any prescribed precision.

389 **4. Numerical Results.** To demonstrate the accuracy and efficiency of the
 390 ATKM, we carry out several numerical experiments. All numerical errors are cal-
 391 culated in the relative maximum norm, defined as follows:

$$392 \quad (4.1) \quad E := \frac{\|\phi - \phi_{\vec{h}}\|_{l^\infty}}{\|\phi\|_{l^\infty}} = \frac{\max_{\mathbf{x} \in \mathcal{T}_h} |\phi(\mathbf{x}) - \phi_{\vec{h}}(\mathbf{x})|}{\max_{\mathbf{x} \in \mathcal{T}_h} |\phi(\mathbf{x})|},$$

393 where \mathcal{T}_h is the rectangular computational domain discretized uniformly in each di-
 394 rection with mesh size vector $\vec{h} = (h_1, \dots, h_d)^T$. Here, the grid function $\phi_{\vec{h}}$ is the
 395 numerical solution and ϕ is the exact/reference solution. We denote the mesh size
 396 vector \vec{h} simply by h if $h_j = h$ for $j = 1, \dots, d$. The algorithm has been implemented
 397 in FORTRAN, and all reported timing results are obtained using a single 2.60GHz
 398 Intel(R) Core(TM) i7-6660U CPU with 4MB cache with the Intel compiler ifort and
 399 optimization level -O3.

400 **4.1. Coulomb potentials.**401 EXAMPLE 1. *The 2D Coulomb potential* ($U(r) = -\frac{1}{2\pi} \ln r$).402 *Case I:* We first test the method with an isotropic Gaussian source $\rho(\mathbf{x}) := e^{-|\mathbf{x}|^2/\sigma^2}$
403 with $\sigma > 0$. The corresponding potential is given by

404 (4.2)
$$\phi(\mathbf{x}) = -\frac{\sigma^2}{4} \left[E_1 \left(\frac{|\mathbf{x}|^2}{\sigma^2} \right) + 2 \ln(|\mathbf{x}|) \right],$$

405 where $E_1(r) := \int_r^\infty t^{-1} e^{-t} dt$ for $r > 0$ is the exponential integral function [39].406 *Case II:* We next consider an anisotropic Gaussian source $\rho(\mathbf{x})$ generated by taking
407 the Laplacian of the potential $\phi(\mathbf{x}) = e^{-\frac{x^2}{\sigma^2} - \frac{y^2}{\alpha^2}}$, $\alpha, \sigma > 0$ as follows:

408 (4.3)
$$\rho(\mathbf{x}) = -\Delta\phi(\mathbf{x}) = \phi(\mathbf{x}) \left(-\frac{4x^2}{\sigma^4} - \frac{4y^2}{\alpha^4} + \frac{2}{\alpha^2} + \frac{2}{\sigma^2} \right).$$

409 Table 4.1 shows the errors for the 2D Coulomb potential with various mesh sizes
410 in Example 1 on $\mathbf{R}_{10\gamma}$ with $\gamma = (1, \gamma)$. For *Case I*, we set $\sigma = \sqrt{1.2}$, $\gamma = 1$ and the
411 mesh size $h_x = h_y = h$, and for *Case II* we set $\sigma = 1.2$, $\alpha = \gamma \sigma$ and $\vec{h} = \frac{1}{4}(1, \gamma)^T$.
412 The saturated accuracy of Case I comes from the Gaussian-sum approximation of the
413 kernel, which could certainly be further improved with more accurate Gaussian-sum
414 approximations if needed.

TABLE 4.1

Errors (E) for the 2D Poisson potential in Example 1 on $\mathbf{R}_{10\gamma}$. For Case I, $\sigma = \sqrt{1.2}$, $\gamma = 1$ and we use a uniform mesh with N points. For Case II, $\sigma = 1.2$, $\alpha = \gamma \sigma$ and we fix $\vec{h} = \frac{1}{4}(1, \gamma)^T$, corresponding to an anisotropic grid with $N = 80 \times 80$ points.

Case I	$N = 10^2$	$N = 20^2$	$N = 40^2$	$N = 80^2$	$N = 160^2$
E	2.180E-01	9.624E-04	5.134E-09	5.854E-11	5.853E-11
Case II	$\gamma = 1$	$\gamma = 1/2$	$\gamma = 1/4$	$\gamma = 1/8$	$\gamma = 1/16$
E	6.767E-13	3.913E-13	2.816E-13	2.299E-13	2.701E-13

415 EXAMPLE 2. *The 3D Coulomb potential restricted to a plane* ($U(r) = \frac{1}{2\pi} \frac{1}{r}$).416 We next consider the anisotropic source $\rho(\mathbf{x}) = e^{-(x^2+y^2/\gamma^2)/\sigma^2}$ with $\sigma > 0$ and $\gamma \leq 1$.
417 The Coulomb potential with targets restricted to the xy -plane is given analytically
418 [6] by

419 (4.4)
$$\phi(\mathbf{x}) = \frac{\gamma \sigma}{\sqrt{\pi}} \int_0^\infty \frac{e^{-\frac{x^2}{\sigma^2(t^2+1)}} e^{-\frac{y^2}{\sigma^2(t^2+\gamma^2)}}}{\sqrt{t^2+1} \sqrt{t^2+\gamma^2}} dt.$$

420 A reference solution is obtained by applying adaptive Gauss–Kronrod quadrature to
421 the above integral and requesting double precision accuracy. The Fourier transform
422 of the isotropically truncated Coulomb kernel with a ball B_D of radius D is given as
423 follows

424 (4.5)
$$\begin{aligned} \widehat{U}_B(\mathbf{k}) &= 2\pi \int_0^D J_0(kr) U(r) r dr = \int_0^D J_0(kr) dr \\ &= \frac{D}{2} (\pi J_1(kD) \text{SH}_0(kD) + J_0(kD) (2 - \pi \text{SH}_1(kD))), \quad k = |\mathbf{k}|, \end{aligned}$$

425 where J_0, J_1 are Bessel functions of the first kind with index 0 and 1, and SH_0, SH_1
 426 are Struve functions of order 0 and 1, respectively [39].

427 A comparison with the TKM for this Coulomb potential is presented in Table 4.2
 428 on the domain $\mathbf{R}_{12\gamma}$ for various anisotropic vectors $\gamma = (1, \gamma)^T$ and mesh size vectors
 429 $\vec{h} = \frac{1}{4}\gamma$. From Table 4.2 one can see clearly that both methods are spectrally accurate,
 430 that the minimum storage required for the TKM depends linearly on the anisotropy
 431 factor $\gamma_f = \gamma$, but that the storage of the ATKM remains unchanged with respect to
 432 γ_f .

TABLE 4.2

Comparison of the ATKM and the TKM for the Coulomb potential in Example 2 on $\mathbf{R}_{L\gamma}$:
 $L = 12, \sigma = 1.5, \vec{h} = \frac{1}{4}(1, \gamma)^T$. N denotes the number of grid points and E denotes the error.

		$\gamma = 1$	$\gamma = 1/2$	$\gamma = 1/4$	$\gamma = 1/8$	$\gamma = 1/16$
ATKM	N	192×192	192×192	192×192	192×192	192×192
	E	1.004E-15	9.738E-16	7.589E-16	1.0572E-15	3.247E-15
TKM	N	192×192	192×384	192×768	192×1536	192×3072
	E	3.353E-16	3.661E-16	3.798E-16	4.531E-16	3.562E-15

433 EXAMPLE 3. The 3D Coulomb potential ($U(r) = \frac{1}{4\pi} \frac{1}{r}$).

434 Let

$$435 \quad \rho_0(\mathbf{x}) := e^{-(x^2+y^2+z^2/\gamma_3^2)/\sigma^2}$$

436 with $\gamma_3 \leq 1$ be an anisotropic Gaussian source distribution. For

$$437 \quad \rho(\mathbf{x}) = \rho_0(\mathbf{x}) + \rho_0(\mathbf{x} - \mathbf{x}_0),$$

438 the corresponding potential is

$$439 \quad \phi(\mathbf{x}) = \phi_0(\mathbf{x}) + \phi_0(\mathbf{x} - \mathbf{x}_0).$$

440 where

$$441 \quad (4.6) \quad \phi_0(\mathbf{x}) = \frac{\gamma_3 \sigma^2}{4} \int_0^\infty \frac{e^{-\frac{x^2+y^2}{\sigma^2(t+1)}} e^{-\frac{z^2}{\sigma^2(t+\gamma_3^2)}}}{(t+1)\sqrt{t+\gamma_3^2}} dt, \quad \mathbf{x} \in \mathbb{R}^3.$$

442 We let $\mathbf{x}_0 = (2, 2, 0)^T$, requiring a 256^3 uniform mesh for resolution to double precision
 443 accuracy.

444 The error and timing results for the ATKM are presented in Table 4.3. Here,
 445 T_{precomp} is the time for the precomputation of \hat{U}_R , and T_{FFT} is the time of the FFT.
 446 The cut-off parameter δ and the number of Gaussian S are also shown.

447 To compare the performance of the TKM and the ATKM, we consider the single
 448 anisotropy Gaussian bump $\rho_0(\mathbf{x}) = e^{-(x^2+y^2+z^2/\gamma_3^2)/\sigma^2}$ and determine the total
 449 number of grid points N needed to achieve the indicated error E in Table 4.4. Fig-
 450 ure 4.1 shows the CPU time in seconds for the TKM and the ATKM as a function
 451 of the anisotropy factor. Clearly, the ATKM is capable of accurate evaluation of
 452 the Coulomb potential without increasing the storage and computation costs as the
 453 anisotropy factor increases. The TKM can be made as accurate as the ATKM, but
 454 the storage and computation costs grow linearly with the anisotropy factor.

TABLE 4.3

Error and timing results of the ATKM for the 3D Coulomb potential (Example 3) on $\mathbf{R}_L\gamma$. Here, $L = 16$, $\sigma = 2$, $\gamma = (1, 1, \gamma_3)$, $\vec{h} = \frac{1}{4}\gamma$. N denotes the number of grid points and E denotes the error. T_{precomp} is the time for precomputing \widehat{U}_R , T_{FFT} is the FFT time. δ is the cut-off parameter and S is the number of Gaussian S used in the kernel approximation.

γ_3	N	E	T_{precomp}	T_{FFT}	δ	S
1	256^3	6.589E-16	3.685	0.8586	4.974E-07	198
1/2	256^3	6.631E-16	3.831	0.8796	2.487E-07	205
1/4	256^3	8.083E-16	3.739	0.8211	1.243E-07	213
1/8	256^3	7.630E-16	3.856	0.8216	6.217E-08	220

TABLE 4.4

Comparison with the TKM for the 3D Coulomb potential with anisotropic Gaussian density (Example 3): $\rho(\mathbf{x}) = e^{-(x^2+y^2+z^2/\gamma_3^2)/\sigma^2}$ on $\mathbf{R}_L\gamma$: $L = 12$, $\sigma = 2$, $\gamma = (1, 1, \gamma_3)^T$ and $\vec{h} = \frac{1}{2}\gamma$. N denotes the number of grid points and E denotes the error.

		$\gamma_3 = 1$	$\gamma_3 = 1/2$	$\gamma_3 = 1/4$	$\gamma_3 = 1/8$	$\gamma_3 = 1/16$
ATKM	N	96^3	96^3	96^3	96^3	96^3
	E	3.522E-15	6.932E-15	1.466E-14	3.021E-14	6.150E-14
TKM	N	96^3	$96^3 \times 2$	$96^3 \times 4$	$96^3 \times 8$	$96^3 \times 16$
	E	3.501E-15	6.957E-15	1.454E-14	2.995E-14	6.200E-14

4.2. Yukawa potentials.

EXAMPLE 4. The 2D Yukawa potential ($U(r) = \frac{1}{2\pi} K_0(\lambda r)$).

Given a potential $\phi(\mathbf{x}) = e^{-\frac{x^2}{\sigma^2} - \frac{y^2}{\delta^2}}$, we define the corresponding density $\rho(\mathbf{x})$ by

$$(4.7) \quad \rho(\mathbf{x}) = \left(\frac{-4x^2\delta^4 - 4y^2\sigma^4 + 2\sigma^2\delta^4 + 2\delta^2\sigma^4}{\sigma^4\delta^4} + \lambda^2 \right) \phi(\mathbf{x}),$$

so that

$$(-\Delta + \lambda^2)\phi(\mathbf{x}) = \rho(\mathbf{x}).$$

We compute the convolution $(U * \rho)[\mathbf{x}]$ using the ATKM to obtain an approximate solution $\phi_{\vec{h}}$. For this, the Fourier transform of the isotropically truncated 2D Yukawa kernel in a ball B_D of radius D is

$$(4.8) \quad \widehat{U}_B(k) = \frac{1}{k^2 + \lambda^2} [1 + k D J_1(kD) K_0(\lambda D) - D \lambda J_0(kD) K_1(\lambda D)],$$

where $K_0(r)$ and $K_1(r)$ are modified Bessel functions of the second kind with order 0 and 1, respectively. In Table 4.5, we present results for the ATKM. As above, the cost remains independent of the anisotropy, whereas it grows linearly with γ_f for the TKM.

EXAMPLE 5. 3D Yukawa potential ($U(r) = \frac{e^{-\lambda r}}{4\pi r}$).

Case I: We consider the isotropic Gaussian source $\rho_0(\mathbf{x}) = e^{-|\mathbf{x}|^2/2\sigma^2}$, $\sigma > 0$, which generates the exact potential [12]

$$(4.9) \quad \phi_0(\mathbf{x}) = \sqrt{2}(\sqrt{\pi}\sigma)^3 \frac{e^{-\lambda r + \frac{\lambda^2\sigma^2}{2}}}{4\pi r} \left[\operatorname{erfc}\left(-\frac{r}{\sqrt{2}\sigma} + \frac{\lambda\sigma}{\sqrt{2}}\right) - e^{2\lambda r} \operatorname{erfc}\left(\frac{r}{\sqrt{2}\sigma} + \frac{\lambda\sigma}{\sqrt{2}}\right) \right],$$

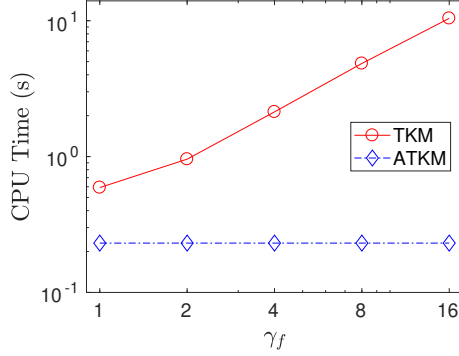


FIG. 4.1. Timing results for the TKM and the ATKM as a function of the anisotropy factor. The data corresponds to experiments carried out for the 3D Coulomb potential (Example 3), described in Table 4.4.

TABLE 4.5

Comparison with the TKM for the 2D Yukawa potential (Example 4) on $\mathbf{R}_{L,\gamma}$: $L = 12$, $\lambda = 1$, $\sigma = \sqrt{1.5}$, $\delta = \gamma\sigma$, $\vec{h} = h\gamma = \frac{1}{4}(1, \gamma)^T$. N denotes the number of grid points and E denotes the error.

		$\gamma = 1$	$\gamma = 1/2$	$\gamma = 1/4$	$\gamma = 1/8$	$\gamma = 1/16$
ATKM	N	192×192	192×192	192×192	192×192	192×192
	E	4.495E-16	3.343E-16	1.615E-16	2.259E-16	6.183E-16
TKM	N	192×192	192×384	192×768	192×1536	192×3072
	E	2.221E-16	2.245E-16	4.463E-16	8.882E-16	1.999E-15

473 where $\text{erfc}(x) = 1 - \frac{2}{\sqrt{\pi}} \int_0^x e^{-t^2} dt$ is the complementary error function. To add some
 474 complexity to the calculation, we consider a density that is composed of multiple such
 475 Gaussians:

$$476 \quad \rho(\mathbf{x}) = \sum_{i,j,k \in \{0,1\}} \rho_0(\mathbf{x} - \mathbf{x}_{ijk}),$$

477 and the potential is given as $\phi(\mathbf{x}) = \sum_{i,j,k \in \{0,1\}} \phi_0(\mathbf{x} - \mathbf{x}_{ijk})$, where $\mathbf{x}_{ijk} = (2^i, 2^j, 3^k)^T$
 478 are shifted centers.

479 *Case II:* Let $\phi(\mathbf{x})$ be given by the anisotropic Gaussian potential

$$480 \quad \phi_0(\mathbf{x}) = e^{-(x^2/\gamma_1^2 + y^2/\gamma_2^2 + z^2/\gamma_3^2)/\sigma^2}, \quad 0 < \gamma_j \leq 1,$$

481 and let

$$482 \quad \rho_0(\mathbf{x}) = - \left(\frac{4x^2}{\gamma_1^4 \sigma^4} - \frac{2}{\gamma_1^2 \sigma^2} + \frac{4y^2}{\gamma_2^4 \sigma^4} - \frac{2}{\gamma_2^2 \sigma^2} + \frac{4z^2}{\gamma_3^4 \sigma^4} - \frac{2}{\gamma_3^2 \sigma^2} - \lambda^2 \right) \phi_0(\mathbf{x}).$$

483 Letting $\phi(\mathbf{x}) = \phi_0(\mathbf{x}) + \phi_0(\mathbf{x} - \mathbf{x}_0)$, it is easy to verify that

$$484 \quad (-\Delta + \lambda^2)\phi(\mathbf{x}) = \rho(\mathbf{x}),$$

485 where $\rho(\mathbf{x}) = \rho_0(\mathbf{x}) + \rho_0(\mathbf{x} - \mathbf{x}_0)$. We compute the convolution $(U * \rho)[\mathbf{x}]$ using the
 486 ATKM to obtain an approximate solution $\phi_{\vec{h}}$ for $\mathbf{x}_0 = (\frac{16}{3}, \frac{8}{3}, 0)^T$.

487 Table 4.6 shows the errors and timing results for the 3D Yukawa potentials in
 488 Example 5.

TABLE 4.6

Error and timing results of the ATKM for the 3D Yukawa potential (Example 5) on $\mathbf{R}_{L\gamma}$ with $\sigma = \frac{1}{4}$. Case I: $L = 12, \vec{h} = h(1, 1, 1)^T$; Case II: $L = 8, \vec{h} = \frac{1}{16}(1, \frac{1}{2}, \gamma_3)^T$. N denotes the number of grid points and E denotes the error. T_{precomp} is the time for precomputing \widehat{U}_R , T_{FFT} is the FFT time. δ is the cut-off parameter and S is the number of Gaussian S used in the kernel approximation.

Case I	N	E	T_{precomp}	T_{FFT}	δ	S
$h = 1/2$	96^3	0.119	0.080	0.027	1.326E-06	104
$h = 1/4$	192^3	1.849E-04	0.814	0.297	6.631E-07	109
$h = 1/8$	384^3	2.996E-12	6.759	2.789	3.316E-07	112
$h = 1/16$	768^3	7.990E-16	41.66	26.32	1.658E-07	116
Case II	N	E	T_{precomp}	T_{FFT}	δ	S
$\gamma_3 = 1$	512^3	1.403E-15	13.98	10.08	1.243E-07	124
$\gamma_3 = 1/2$	512^3	7.400E-16	17.92	9.651	1.243E-07	124
$\gamma_3 = 1/4$	512^3	2.296E-15	15.75	10.06	6.217E-08	129
$\gamma_3 = 1/8$	512^3	5.161E-15	18.07	9.677	3.108E-08	134
$\gamma_3 = 1/16$	512^3	4.502E-15	16.93	9.866	1.554E-08	139

4.3. Biharmonic potentials.

EXAMPLE 6. The 2D biharmonic potential ($U(r) = -\frac{1}{8\pi} r^2(\log(r) - 1)$).

Case I: We consider the isotropic Gaussian source

$$\rho(\mathbf{x}) = \frac{1}{2\pi\sigma^2} e^{-\frac{|\mathbf{x}|^2}{2\sigma^2}}, \quad \mathbf{x} \in \mathbb{R}^2,$$

which generates the exact potential

$$\phi(\mathbf{x}) = \frac{1}{8\pi} \left(r^2 + e^{-\frac{r^2}{2\sigma^2}} \sigma^2 \right) + \frac{1}{16\pi} (r^2 + 2\sigma^2) \left(\text{Ei} \left(-\frac{r^2}{2\sigma^2} \right) - 2 \log(r) \right),$$

where $r = |\mathbf{x}|$ and $\text{Ei}(x) := \int_{-\infty}^x \frac{e^s}{s} ds$ is the exponential integral [39].

Case II: Let the exact solution $\phi(\mathbf{x})$ be given by the anisotropic Gaussian potential

$\phi(\mathbf{x}) = e^{-(x^2/\gamma_1^2 + y^2/\gamma_2^2)/\sigma^2}$, $0 < \gamma_j \leq 1, j = 1, 2$, and let

$$\rho(\mathbf{x}) = -\Delta^2 \phi(\mathbf{x}).$$

Numerical results are presented in Table 4.7. Spectral convergence is evident until

the error in the kernel approximation using a sum of Gaussians begins to dominate.

TABLE 4.7

Errors (E) for the 2D biharmonic potential in Example 6 on $\mathbf{R}_{L\gamma}$. For Case I, $L = 12, \sigma = \sqrt{1.2}$ and we use a uniform mesh with N points. For Case II, $L = 10, \sigma = 1.2, \gamma = (1, \gamma)^T$ and we fix $\vec{h} = \frac{1}{4}(1, \gamma)^T$, corresponding to an anisotropic grid with $N = 80 \times 80$ points.

Case I	$N = 48^2$	$N = 96^2$	$N = 128^2$	$N = 256^2$
E	9.333E-03	7.516E-07	3.172E-11	3.172E-11
Case II	$\gamma = 1$	$\gamma = 1/2$	$\gamma = 1/4$	$\gamma = 1/8$
E	1.604E-10	5.305E-10	1.767E-09	8.482E-09

EXAMPLE 7. The 3D biharmonic potential ($U(r) = \frac{r}{8\pi}$).

Case I: We consider the isotropic Gaussian source

$$\rho(\mathbf{x}) = \frac{1}{(2\pi)^{3/2}\sigma^3} e^{-\frac{|\mathbf{x}|^2}{2\sigma^2}}, \quad \mathbf{x} \in \mathbb{R}^3,$$

500 which generates the exact potential [12]

$$501 \quad \phi(\mathbf{x}) = \frac{1}{8\pi} \left(\operatorname{Erf} \left(\frac{r}{\sqrt{2}\sigma} \right) \left(\frac{\sigma^2}{r} + r \right) + \sigma \sqrt{\frac{2}{\pi}} e^{-\frac{r^2}{2\sigma^2}} \right), \quad r = |\mathbf{x}|.$$

502 Case II: Let $\phi(\mathbf{x})$ be given by the anisotropic Gaussian potential

$$503 \quad \phi(\mathbf{x}) = e^{-(x^2/\gamma_1^2 + y^2/\gamma_2^2 + z^2/\gamma_3^2)/\sigma^2}, \quad 0 < \gamma_j \leq 1,$$

504 and let

$$505 \quad \rho(\mathbf{x}) = -\Delta^2 \phi(\mathbf{x}).$$

506 We compute the convolution $(U * \rho)[\mathbf{x}]$ using the ATKM to obtain an approximate
507 solution $\phi_{\vec{h}}$.

508 Table 4.8 presents the errors and timing results for the 3D biharmonic potentials
509 in Example 7.

TABLE 4.8

Error and timing results of the 3D biharmonic potential (Example 7) on $\mathbf{R}_{L,\gamma}$ with $\sigma = \sqrt{1.2}$.
Case I: $L = 12, \gamma = (1, 1, 1)^T, \vec{h} = h\gamma$; Case II: $L = 10, \gamma = (1, \frac{1}{4}, \gamma_3)^T$ and $\vec{h} = \frac{1}{4}\gamma$. N denotes
the number of grid points and E denotes the error. T_{precomp} is the time for precomputing \hat{U}_R , T_{FFT}
is the FFT time. δ is the cut-off parameter and S is the number of Gaussian S used in the kernel
approximation.

Case I	N	E	T_{precomp}	T_{FFT}	δ	S
$h = 1$	48^3	1.585E-02	9.700E-03	5.000E-04	5.305E-06	199
$h = 1/2$	96^3	5.962E-07	4.070E-02	2.900E-03	2.653E-06	199
$h = 1/4$	192^3	1.031E-11	2.373E-01	2.800E-02	1.326E-06	203
$h = 1/8$	384^3	1.701E-11	1.809	3.356E-01	6.631E-07	213
Case II	N	E	T_{precomp}	T_{FFT}	δ	S
$\gamma_3 = 1$	160^3	5.499E-12	1.057	0.176	1.989E-07	213
$\gamma_3 = 1/2$	160^3	3.692E-12	1.070	0.168	1.989E-07	213
$\gamma_3 = 1/4$	160^3	3.260E-12	1.060	0.184	1.989E-07	213
$\gamma_3 = 1/8$	160^3	1.873E-11	1.064	0.169	9.947E-08	213

510 **4.4. Application to anisotropic layered media.** We consider the transmis-
511 sion problem (see Figure 4.2)

$$512 \quad (4.9) \quad -\nabla \cdot (\varepsilon_i \nabla \phi) = f_i, \quad i = 1, 2,$$

513 subject to continuity conditions at the interface, i.e., at the xy -plane ($z = 0$)

$$514 \quad (4.10) \quad \begin{aligned} [\phi] &:= \phi(x, y, 0+) - \phi(x, y, 0-) = 0, \\ [\varepsilon \partial_{\mathbf{n}} \phi] &:= \varepsilon_1 \phi_z(x, y, 0+) - \varepsilon_2 \phi_z(x, y, 0-) = 0, \end{aligned}$$

515 where ε_i ($i = 1, 2$) are constants and the source terms f_1, f_2 are given smooth and
516 rapidly decaying functions with (numerical) compact support in regions I and II , re-
517 spectively. We will consider source densities that are strongly anisotropic, in the sense

518 that their extent in the z -direction is very small compared to their extents in the x and
 519 y directions. One such example density is $f_1(\mathbf{x}) = e^{-((x-x_0)^2+(y-y_0)^2+(z-z_0)^2)/\eta^2}/\sigma^2$
 520 with $\eta \ll 1$.

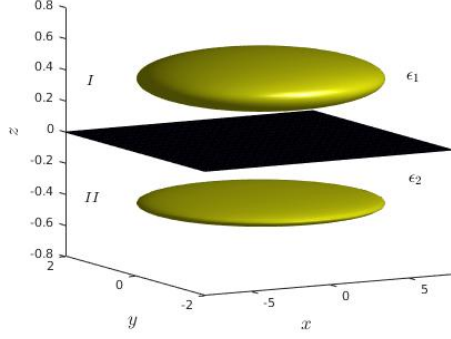


FIG. 4.2. Schematic of the anisotropic layered problem.

521 We first decompose ϕ into two parts using standard potential theory. That is,
 522 $\phi = \phi^F + \phi^S$, where ϕ^F is the volume potential due to the inhomogeneous source
 523 terms

$$524 \quad (4.11) \quad \phi^F(\mathbf{x}) = \begin{cases} \frac{1}{4\pi|\mathbf{x}|} * \frac{f_1}{\varepsilon_1}, & \mathbf{x} \in I, \\ \frac{1}{4\pi|\mathbf{x}|} * \frac{f_2}{\varepsilon_2}, & \mathbf{x} \in II. \end{cases}$$

525 We apply the ATKM to calculate ϕ^F on a uniform grid. In order for ϕ to satisfy the
 526 continuity conditions above, we let ϕ^S denote a correction term which satisfies the
 527 Laplace equation in both the upper and lower half-spaces with suitable decay condi-
 528 tions at infinity. It is well-known that ϕ^S can be represented using a ‘‘Sommerfeld-
 529 type’’ integral [38] of the form

$$530 \quad \phi^S(\mathbf{x}) = \begin{cases} \frac{1}{(2\pi)^2} \int_0^\infty e^{-kz} dk \int_0^{2\pi} M_1(k, \beta) e^{ik(x \cos \beta + y \sin \beta)} d\beta, & z > 0, \\ \frac{1}{(2\pi)^2} \int_0^\infty e^{kz} dk \int_0^{2\pi} M_2(k, \beta) e^{ik(x \cos \beta + y \sin \beta)} d\beta, & z < 0, \end{cases}$$

531 Here, M_1 and M_2 are unknown densities to be determined.

532 Direct application of (4.10) leads to a 2×2 linear system for each point (k, β) .

$$533 \quad (4.12) \quad \begin{cases} M_1 - M_2 = k g_1, \\ \varepsilon_1 M_1 + \varepsilon_2 M_2 = -g_2, \end{cases} \implies \begin{cases} M_1 = \frac{1}{\varepsilon_1 + \varepsilon_2} (\varepsilon_2 k g_1 - g_2), \\ M_2 = \frac{1}{\varepsilon_1 + \varepsilon_2} (-\varepsilon_1 k g_1 - g_2), \end{cases}$$

534 where

$$535 \quad (4.13) \quad g_1(k, \beta) := -\frac{1}{2\pi} \int_{\mathbb{R}} \frac{\widehat{f}_1(k, \beta, k_3)/\varepsilon_1 - \widehat{f}_2(k, \beta, k_3)/\varepsilon_2}{k^2 + k_3^2} dk_3,$$

$$536 \quad (4.14) \quad g_2(k, \beta) := -\frac{1}{2\pi} \int_{\mathbb{R}} \frac{(\widehat{f}_1(k, \beta, k_3) - \widehat{f}_2(k, \beta, k_3)) i k_3}{k^2 + k_3^2} dk_3,$$

537 using cylindrical coordinates (k, β, k_3) .

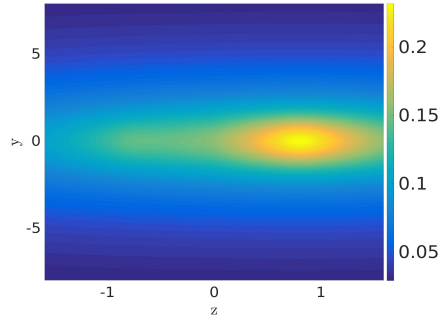


FIG. 4.3. Potential in the plane $x = 0$, i.e., $\phi(0, y, z)$.

538 For each (k, β) , we compute kg_1 and g_2 using adaptive Gauss-Kronrod quadrature.
 539 Once M_1 and M_2 are obtained from (4.12), $\phi^S(\mathbf{x})$ is then evaluated using the NUFFT-
 540 based method of [5, 27].

541 In our example, we set $\varepsilon_1 = 1$, $\varepsilon_2 = 2$, and

$$542 \quad f_i(\mathbf{x}) = e^{-\frac{(x-x_i)^2}{\sigma_{i,x}^2} - \frac{(y-y_i)^2}{\sigma_{i,y}^2} - \frac{(z-z_i)^2}{\sigma_{i,z}^2}}, \quad i = 1, 2,$$

543 with $\vec{\sigma}_1 = (2.5, 1.1, 0.2)^T$, $\vec{\sigma}_2 = (2.5, 1.1, 0.1)^T$ and the centers $\mathbf{x}_1 = (x_1, y_1, z_1)^T =$
 544 $(0, 0, 0.8)^T$, $\mathbf{x}_2 = (0, 0, -0.8)^T$. The computational domain is chosen to be $[-8, 8]^2 \times$
 545 $[0, 1.6]$ for region *I* and $[-8, 8]^2 \times [-1.6, 0]$ for region *II*, respectively. The mesh sizes
 546 are set to be $h_x = h_y = \frac{1}{8}$ and $h_z = \frac{1}{80}$ in both regions. In Figure 4.3, we plot the
 547 potential as a function of y and z in the plane $x = 0$. Numerical convergence tests
 548 indicate that at least 10 digits of accuracy are obtained with a $128 \times 128 \times 256$ grid.

549 **5. Conclusion.** We have developed a new method – the anisotropic truncated
 550 kernel method (ATKM) for computing nonlocal potentials that are convolutions of a
 551 radially symmetric kernel with a smooth and rapidly decaying source density. When
 552 the density has compact support on an *anisotropic* rectangular box $\mathbf{R}_{L\gamma}$, the kernel
 553 is truncated on a rectangular box $\mathbf{R}_{2L\gamma}$ that doubles the length of each side. The
 554 potential is then computed via the FFT with an optimal zero-padding factor (2^d) for
 555 problems in d dimensions. The method is a useful extension of the isotropic kernel
 556 truncation method in [49], since it avoids excessive zero-padding for highly anisotropic
 557 problems and reduces the cost by a factor of γ_f (see Definition (1.5)).

558 A fast algorithm is required to obtain the Fourier transform of the anisotropically
 559 truncated kernel. For this, we used a sum-of-Gaussians approximation of the kernel
 560 away from the origin plus a local correction to handle the singularity at the origin.
 561 The Gaussian-sum approximation is obtained either via a spectral discretization of an
 562 integral representation of the kernel (when available), or via a black-box algorithm in
 563 the general case. The algorithm applies to nonoscillatory kernels, including many of
 564 the kernels encountered in mathematical physics and engineering. We are currently
 565 investigating oscillatory problems such as the Helmholtz equation, and will report our
 566 findings at a later date.

- 568 [1] J. C. AGUILAR AND Y. CHEN, *High-Order Corrected Trapezoidal Quadrature Rules for Func-*
569 *tions with a Logarithmic Singularity in 2-D*, *Comput. Math. Appl.*, 44 (2002), pp. 1031–
570 1039.
- 571 [2] J. C. AGUILAR AND Y. CHEN, *High-order corrected trapezoidal quadrature rules for the coulomb*
572 *potential in three dimensions*, *Comput. Math. Appl.*, 49 (2005), pp. 625–631.
- 573 [3] W. BAO, Y. CAI, AND H. WANG, *Efficient numerical methods for computing ground states and*
574 *dynamics of dipolar Bose-Einstein condensates*, *J. Comput. Phys.*, 229 (2010), pp. 7874–
575 7892.
- 576 [4] W. BAO, H. JIAN, N. MAUSER, AND Y. ZHANG, *Dimension reduction of the Schrödinger equa-*
577 *tion with Coulomb and anisotropic confining potentials*, *SIAM J. Appl. Math.*, 73 (2010),
578 pp. 7874–7892.
- 579 [5] W. BAO, S. JIANG, Q. TANG, AND Y. ZHANG, *Computing the ground state and dynamics of*
580 *the nonlinear Schrödinger equation with nonlocal interactions via the nonuniform FFT*, *J.*
581 *Comput. Phys.*, 296 (2015), pp. 72–89.
- 582 [6] W. BAO, Q. TANG, AND Y. ZHANG, *Accurate and efficient numerical methods for computing*
583 *ground states and dynamics of dipolar Bose-Einstein condensates via the nonuniform FFT*,
584 *Comm. Comput. Phys.*, 19 (2016), pp. 1141–1166.
- 585 [7] J. T. BEALE AND M.-C. LAI, *A method for computing nearly singular integrals*, *SIAM J. Numer.*
586 *Anal.*, 38 (2001), pp. 1902–25.
- 587 [8] C. BERTOGLIO AND B. N. KHOROMSKIJ, *Low-rank quadrature-based tensor approximation of the*
588 *Galerkin projected Newton/Yukawa kernels*, *Comput. Phys. Comm.*, 183 (2012), pp. 904–
589 912.
- 590 [9] G. BEYLKIN, C. KURZC, AND L. MONZÓN, *Fast convolution with the free space Helmholtz*
591 *Green’s function*, *J. Comput. Phys.*, 228 (2009), pp. 2770–2791.
- 592 [10] G. BEYLKIN AND L. MONZÓN, *Approximation by exponential sums*, *Appl. Comput. Harmon.*
593 *Anal.*, 19 (2005), pp. 17–48.
- 594 [11] G. BEYLKIN AND L. MONZÓN, *Approximation by exponential sums revisited*, *Appl. Comput.*
595 *Harmon. Anal.*, 28 (2010), pp. 131–149.
- 596 [12] A. CERIONI, L. GENOVESE, A. MIRONE, AND V. SOLE, *Efficient and accurate solver of the three-*
597 *dimensional screened and unscreened Poisson’s equation with generic boundary conditions*,
598 *J. Chem. Phys.*, 137 (2012), p. 134108.
- 599 [13] T. DARDEN, D. YORK, AND L. PEDERSEN, *Particle mesh ewald - an $o(n \log n)$ method for Ewald*
600 *sums in large systems*, *J. Chem. Phys.*, 98 (1993), pp. 10089–10092.
- 601 [14] R. DUAN AND V. ROKHLIN, *High-order quadratures for the solution of scattering problems in two*
602 *dimensions*, *J. Comput. Phys.*, 228 (2009), pp. 2152–2174, doi:10.1016/j.jcp.2008.11.033.
- 603 [15] A. DUTT AND V. ROKHLIN, *Fast Fourier transforms for nonequispaced data*, *SIAM J. Sci.*
604 *Comput.*, 14 (1993), pp. 1368–1393.
- 605 [16] F. ETHRIDGE AND L. GREENGARD, *A New Fast-Multipole Accelerated Poisson Solver in Two*
606 *Dimensions*, *SIAM J. Sci. Comput.*, 23 (2001), pp. 741–760.
- 607 [17] L. EXL, N. MAUSER, AND Y. ZHANG, *Accurate and efficient computation of nonlocal potentials*
608 *based on Gaussian-sum approximation*, *J. Comput. Phys.*, 327 (2016), pp. 629–642.
- 609 [18] L. FÜSTI-MOLNAR AND P. PULAY, *Accurate molecular integrals and energies using combined*
610 *plane wave and Gaussian basis sets in molecular electronic structure theory*, *J. Chem.*
611 *Phys.*, 116 (2002), p. 7795.
- 612 [19] W. GAUTSCHI, *Efficient computation of the complex error function*, *SIAM J. Numer. Anal.*, 7
613 (1970), pp. 187–198.
- 614 [20] L. GENOVESE, T. DEUTSCH, AND S. GOEDECKER, *Efficient and accurate three-dimensional*
615 *Poisson solver for surface problems*, *J. Chem. Phys.*, 127 (2007), p. 054704.
- 616 [21] L. GENOVESE, T. DEUTSCH, A. NEELOV, S. GOEDECKER, AND G. BEYLKIN, *Efficient solution*
617 *of Poisson equation with free boundary conditions*, *J. Chem. Phys.*, 125 (2006), p. 074105.
- 618 [22] K. GLOVER, *All optimal Hankel-norm approximations of linear multivariable systems and their*
619 *l^∞ -error bounds*, *Int. J. Control*, 39 (1984), pp. 1115–1193.
- 620 [23] J. GOODMAN, T. Y. HOU, AND J. LOWENGRUB, *The convergence of the point vortex method for*
621 *the 2-D Euler equations*, *Commun. Pur. Appl. Math.*, 43 (1990), pp. 415–430.
- 622 [24] L. GREENGARD AND J. Y. LEE, *Accelerating the nonuniform fast Fourier transform*, *SIAM*
623 *Rev.*, 46 (2004), pp. 443–454.
- 624 [25] W. HACKBUSCH AND B. KHOROMSKIJ, *Low-rank Kronecker-product approximation to multi-*
625 *dimensional nonlocal operators. Part I. Separable approximation of multi-variate func-*
626 *tions*, *Computing*, 76 (2006), pp. 177–202.
- 627 [26] M. R. JARVIS, I. D. WHITE, R. W. GODBY, M. C. PAYNE, AND A. RUBIO, *Supercell technique*
628 *for total-energy calculations of finite charged and polar systems*, *Phys. Rev. B*, 56 (1997),
629 p. 14972.

- 630 [27] S. JIANG, L. GREENGARD, AND W. BAO, *Fast and accurate evaluation of nonlocal Coulomb*
631 *and dipole-dipole interactions via the nonuniform FFT*, SIAM J. Sci. Comput., 36 (2014),
632 pp. B777–B794.
- 633 [28] S. JIANG AND Y. ZHANG, *A black-box algorithm for efficient and accurate sum-of-exponential*
634 *approximation of certain class of functions on an interval*. in preparation, 2018.
- 635 [29] S. G. JOHNSON, *Faddeeva Package*. [http://ab-initio.mit.edu/wiki/index.php/Faddeeva-](http://ab-initio.mit.edu/wiki/index.php/Faddeeva_Package)
636 [Package](http://ab-initio.mit.edu/wiki/index.php/Faddeeva_Package), 2012.
- 637 [30] H. LANGSTON, L. GREENGARD, AND D. ZORIN, *A free-space adaptive fmm-based pde solver in*
638 *three dimensions*, Comm. Appl. Math. and Comp. Sci., 6 (2011), pp. 79–122.
- 639 [31] H. LEE, T. DARDEN, AND L. PEDERSEN, *Accurate crystal molecular dynamics simulations using*
640 *Particle-Mesh-Ewald*, Chemical Physics Letters, 243 (1995), pp. 229–235.
- 641 [32] D. LINDBO AND A.-K. TORNBORG, *Spectral accuracy in fast Ewald-based methods for particle*
642 *simulations*, J. Comput. Phys., 230 (2011), pp. 8744–8761.
- 643 [33] J. LOWENGRUB, M. SHELLEY, AND B. MERRIMAN, *High-order and efficient methods for the*
644 *vorticity formulation of the Euler equations*, SIAM J. Sci. Comput., 14 (1993), pp. 1107–
645 1142.
- 646 [34] D. MALHOTRA AND G. BIROS, *A parallel kernel independent fmm for particle and volume*
647 *potentials*, Commun. Comput. Phys., 18 (2015), pp. 808–830.
- 648 [35] G. MARTYNA AND M. TUCKERMAN, *A reciprocal space based method for treating long range*
649 *interactions in ab initio and force-field-based calculations in clusters*, J. Chem. Phys., 110
650 (1999), pp. 2810–2821.
- 651 [36] N. MAUSER, H. STIMMING, AND Y. ZHANG, *A novel nonlocal potential solver based on nonuni-*
652 *form FFT for efficient simulation of the Davey-Stewartson equations*, ESAIM: Math.
653 Model. Numer. Anal., 51 (2017), pp. 1527–1538.
- 654 [37] P. MCCORQUODALE, P. COLELLA, G. T. BALLS, AND S. B. BADEN, *A scalable parallel pois-*
655 *son solver in three dimensions with infinite-domain boundary conditions*, in In 7th In-
656 *ternational Workshop on High Performance Scientific and Engineering Computing*, 2005,
657 pp. 814–822.
- 658 [38] P. MORSE AND H. FESHBACH, *Methods of Theoretical Physics*, McGraw-Hill, New York, NY,
659 1953.
- 660 [39] F. W. J. OLVER, D. W. LOZIER, R. F. BOISVERT, AND C. W. CLARK, eds., *NIST Handbook of*
661 *Mathematical Functions*, Cambridge University Press, May 2010, <http://dlmf.nist.gov>.
- 662 [40] J. PHILLIPS AND J. WHITE, *A Precorrected-FFT method for capacitance extraction of compli-*
663 *cated 3-D structures*, in Int. Conf. On Computer-Aided Design, Santa Clara, 1994.
- 664 [41] J. PHILLIPS AND J. WHITE, *A precorrected-FFT method for electrostatic analysis of complicated*
665 *3-D structures*, IEEE Trans. Computer-Aided Design, 16 (1997), pp. 1059–1072.
- 666 [42] G. P. M. POPPE AND C. M. J. WIJERS, *More efficient computation of the complex error*
667 *function*, ACM Trans. Math. Soft., 16 (1990), pp. 38–46.
- 668 [43] C. A. ROZZI, D. VARSANO, A. MARINI, E. K. U. GROSS, AND A. RUBIO, *Exact Coulomb cutoff*
669 *technique for supercell calculations*, Phys. Rev. B, 73 (2006), p. 205119.
- 670 [44] W. RUDIN, *Functional Analysis*, McGraw-Hill, New York, second ed., 1991.
- 671 [45] D. S. SHAMSHIRGAR AND A.-K. TORNBORG, *Fast ewald summation for electrostatic potentials*
672 *with arbitrary periodicity*, arXiv:1712.04732, (2017).
- 673 [46] A.-K. TORNBORG, *The Ewald sums for singly, doubly and triply periodic electrostatic systems*,
674 *Adv. Comput. Math.*, 42 (2016), pp. 227–248.
- 675 [47] L. TREFETHEN, *Spectral Methods in Matlab*, Oxford University, 2000.
- 676 [48] G. VAINIKKO, *Fast solvers of the Lippmann-Schwinger equation*, Direct and Inverse Problems
677 of Mathematical Physics, 5 (2000), pp. 423–440.
- 678 [49] F. VICO, L. GREENGARD, AND M. FERRANDO, *Fast convolution with free-space Green’s func-*
679 *tions*, J. Comput. Phys., 323 (2016), pp. 191–203.
- 680 [50] J. WHITE, J. PHILLIPS, AND T. KORSMEYER, *Comparing Precorrected-FFT and fast multipole*
681 *algorithms for solving three-dimensional potential integral equations*, in Proceedings of the
682 *Colorado Conference on Iterative Methods*, Breckenridge, Colorado, 1994.
- 683 [51] K. XU AND S. JIANG, *A bootstrap method for sum-of-poles approximations*, J. Sci. Comput., 55
684 (2013), pp. 16–39.
- 685 [52] M. R. ZAGHLOUL AND A. N. ALI, *Algorithm 916: Computing the Faddeyeva and Voigt func-*
686 *tions*, ACM Trans. Math. Soft., 38 (2011), p. 15.